



Full Length Article

Chemical kinetic basis of synergistic blending for research octane number



Gina M. Fioroni^{a,*}, Mohammad J. Rahimi^{a,1}, Charles K. Westbrook^b, Scott W. Wagnon^b, William J. Pitz^b, Seonah Kim^{a,c}, Robert L. McCormick^a

^a National Renewable Energy Laboratory, Golden, CO 80401, United States

^b Lawrence Livermore National Laboratory, Livermore, CA 94550, United States

^c Colorado State University, Fort Collins, CO 80523, United States

ARTICLE INFO

Keywords:

Octane number
Nonlinear blending
Combustion kinetics
Ethanol
Furans
Prenol

ABSTRACT

Utilizing kinetic simulations with the Co-Optimization of Fuels & Engines (Co-Optima) mechanism, the research octane number (RON) of various synergistic blendstocks at several blend levels in a four-component surrogate were predicted and compared against measured values. The blendstocks investigated include dimethylfuran (DMF), 2-methylfuran (2MF), prenil, 2-methyl-2-butene (2M2B), and ethanol—selected because of their nonlinear blending or synergistic behavior. The RON predictions are in excellent agreement with measured values for DMF and ethanol (within 2 RON units), with less satisfying results for 2MF and 2M2B (as much as 6 and 12 RON units off respectively). The predictions for prenil do not even capture the synergistic blending behavior observed experimentally, reflecting the fact that the kinetic model for prenil does not include sufficiently accurate low-temperature chemistry. The kinetic model was interrogated to understand the most important reactions consuming the blendstock and surrogate components, to understand the most important reactions responsible for the synergistic blending behavior. Better synergistic blenders scavenge hydroxyl radicals (OH) by addition reactions rather than hydrogen-abstraction (H-abstraction) reactions. In addition, those blendstocks, such as 2M2B, can form resonance-stabilized radical products, leading to superior RON boosting compared to ethanol. DMF and 2MF were shown to have the highest RON-boosting ability due to the rapid reaction of the OH addition products to other species that pull the OH addition equilibrium toward products.

1. Introduction

Knock in a spark-ignition (SI) engine is caused by autoignition of the unburnt fuel–air mixture ahead of the spark-ignited propagating flame front and can cause engine damage if severe or allowed to occur over a long period of time. The occurrence of knock limits the ability to operate at optimal combustion phasing (optimal efficiency) with increased compression ratio, engine boosting and downsizing, and other strategies for improving efficiency [1]. Octane number is a measure of resistance to autoignition, which means resistance to knock within the context of spark-ignition engines. There are two octane numbers, the research octane number (RON) and the motor octane number (MON) that were developed historically to predict knock resistance at different engine operating conditions [2]. In modern engines RON is much more closely

correlated with knock-limited operation [1,3] such that RON is a critical property of SI engine fuels and is the most important property for enabling higher-efficiency engine designs [3]. Octane sensitivity (the difference between RON and motor octane number [MON]), the heat of vaporization, flame speed, and other fuel properties are also important, but here we consider only RON.

RON (or MON) is measured in a Cooperative Fuels Research (CFR) engine, which is a single cylinder engine with variable compression ratio developed specifically for this measurement [4]. Mixtures of n-heptane and isooctane (2,2,4-trimethylpentane) are used as primary reference fuels (PRF) to define the octane number scale. N-heptane defines zero on the scale while isooctane defines 100. For mixtures of these components, the isooctane volume percent is the octane number. For example, a mixture of 90 vol% isooctane and 10 vol% n-heptane has an octane

Abbreviations: 2M2B, 2-methyl-2-butene; 2MF, 2-methylfuran; BOB, blendstock for oxygenate blending; CAD, crank-angle degree; Co-Optima, Co-Optimization of Fuels & Chemicals; DMF, 2,5-dimethylfuran; MON, motor octane number; NPR, net progress rate; PRF, primary reference fuel; RON, research octane number; RSR, resonance-stabilized radicals; SI, spark ignition.

* Corresponding author.

E-mail address: gina.fioroni@nrel.gov (G.M. Fioroni).

¹ Equally contributing author.

<https://doi.org/10.1016/j.fuel.2021.121865>

Received 2 July 2021; Received in revised form 25 August 2021; Accepted 27 August 2021

Available online 9 September 2021

0016-2361/© 2021 The Author(s).

Published by Elsevier Ltd.

This is an open access article under the CC BY-NC-ND license

(<http://creativecommons.org/licenses/by-nc-nd/4.0/>).

number of 90 and is referred to as PRF 90. For a given test fuel, the compression ratio is adjusted to obtain a predefined level of knock intensity. The PRF that yields the same knock intensity at this compression ratio has the same octane number as the test fuel.

Commercial gasolines are a mixture of many individual compounds and may include specific bio-blendstocks such as ethanol to reduce emissions and increase octane number [5]. Many individual compounds and blendstocks are known to blend synergistically for RON [6]. Such components do not blend according to a volumetric or molar linear blending model and produce higher RON values than are predicted according to linear models. This is a significant advantage for the fuel blender in that a lower volume of the blendstock is required to meet an octane number target, or a potentially lower-cost, lower-octane-number petroleum refinery base blendstock can be employed. Nonlinear blending may lead to false negatives or false positives when screening prospective blendstocks based on their pure component octane number values. The research reported here uses molar concentrations and molar blending models rather than volumetric blending, as is common in the petroleum refining industry, because a chemical kinetic analysis for nonlinear blending will be most meaningful on this basis.

Previously, researchers measured the RON of 20 potential bioderived blendstocks blended into a four-component gasoline surrogate described in Table 1 [6]. Many blendstocks including alcohols, olefins, and alkylfurans blended synergistically. Because of ethanol's importance in the marketplace, many studies have examined its synergistic blending in petroleum refinery blendstocks and gasoline surrogates. Fig. 1 shows measured RON results for ethanol, along with the expected RON for linear molar blending. Equation (1) shows the simple molar blending model for RON:

$$RON_{blend} = X_{bob} \cdot RON_{bob} + X_{bstk} \cdot RON_{bstk} \quad (1)$$

where:

RON_{blend} is the measured RON of the blend

X_{bob} is the mole fraction of the refinery blendstock or surrogate—based on average molecular weight)

RON_{bob} is the measured RON of the refinery blendstock or surrogate

X_{bstk} is the mole fraction of the added blendstock

RON_{bstk} is the measured RON of the added blendstock

The refinery blendstocks that are blended with ethanol to make commercial gasoline are referred to as blendstock for oxygenate blending (BOB) because they do not meet ASTM or regulatory requirements for finished gasoline until blended with ethanol. In particular, a refinery BOB will typically have an octane number that is too low to meet market requirements (a sub-octane BOB) until blended with ethanol. Ethanol blending is the most well-known example of synergistic blending where measured results are higher than predicted by a linear model, and by a margin that is clearly outside the range of the experimental uncertainty. The reproducibility of the RON measurement is described in the ASTM method (D2699). For the range of 90.0–100.0 the difference between two results obtained on identical test samples would exceed 0.7 O.N. only in one case in twenty. We have interpreted this as a 95% confidence interval of ± 0.7 . For higher values of RON the confidence intervals are:

- 101.0 \pm 1
- 102.0 \pm 1.4
- 103.0 \pm 1.7

Table 1

Composition of four-component surrogate [6]; RON = 90.3, MON = 84.7.

Species	Liquid Volume fraction	Mass fraction	Mole fraction
Isooctane	0.55	0.519	0.469
Toluene	0.25	0.296	0.331
n-Heptane	0.15	0.140	0.144
1-Hexene	0.05	0.046	0.056

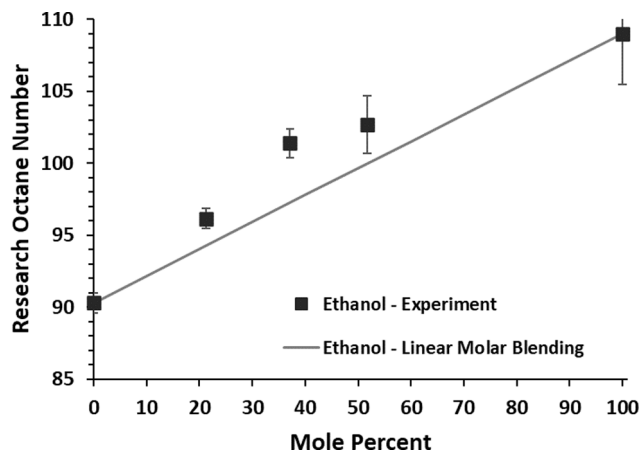


Fig. 1. Measured RON and RON predicted from a linear molar blending model for ethanol blends. Ethanol blended into a four-component surrogate [6].

- 104 \pm 2
- >104 to 108 \pm 3.5

Research on ethanol blending reveals that synergistic blending arises from the interaction between the BOB and ethanol, such that the degree of synergy observed depends on BOB chemical composition. Anderson et al. [7], and later Badra et al. [8] used the difference between measured RON and predicted RON by a linear molar blending model to describe nonlinear blending effects for ethanol in the development of empirical models to predict RON. Anderson et al. [5] suggested that this difference was primarily caused by the interaction of ethanol with isoparaffins and referred to it as ON_{int} , or the total octane number increase from interactions between ethanol and the hydrocarbon fuel. Badra et al. used the difference between measured RON and the linear molar blending predicted values and measured this difference for blends of ethanol into several specific hydrocarbon compounds [8]. Foong et al. [9] showed that ethanol blends synergistically with n-heptane, isooctane, and their blends (primary reference fuels [PRF]) but antagonistically with toluene (antagonistic blending occurs when the blend RON is less than that predicted by a linear molar blending model). In the most recent empirical modeling study of 280 commercial gasolines, Anderson and Wallington [10] use an interaction parameter that can be equally correlated with the fractions of saturates and aromatics or octane sensitivity. Taken together, these studies indicate that ethanol synergistic blending is caused by interaction with the autoignition of paraffins and isoparaffins—species that can undergo low-temperature autoignition. This is well aligned with the conclusion of others that in the synergistic blending of ethanol with PRF, ethanol reacts with hydroxyl radical (OH) generated from paraffin low-temperature autoignition, ultimately yielding much less reactive HO_2 radicals and acetaldehyde [11,12].

No other synergistic blending species have been examined at the level of detail of ethanol. However, some studies have examined isobutanol and 2-methylfuran (2MF). Isobutanol blending into 34 commercial BOBs was examined to develop an empirical blending model [13]. The results showed that isobutanol blended synergistically with paraffins but antagonistically with olefins and aromatics. Both 2MF and 2,5-dimethylfuran (DMF) have been observed in several studies to have a significantly larger synergistic effect than ethanol or isobutanol [6,14,15]. Singh et al. [15] examined blends of 2MF into PRF60 and showed much greater suppression of low-temperature reaction chemistry than observed for ethanol, suggesting that 2MF was an even better OH radical scavenger as discussed in more detail later in Section 3.4 *Kinetic Simulations – Dimethylfuran and 2-Methylfuran*. Tripathi et al. [16] developed a chemical kinetic model for the oxidation of 2MF and 2MF-heptane blends. They showed that under low-temperature conditions

(690 K), 2MF competes with n-heptane for the OH radicals formed in chain branching reactions and that OH addition to the ring was the dominant 2MF consumption pathway. More recently, Shankar et al. [17] used kinetic simulations to show that for 2MF, OH addition to the furan ring is much faster than H-abstraction reactions from hydrocarbons at low temperatures and that this initial OH addition product rapidly reacts to form the ring opening product, driving the OH addition reaction forward. They also showed that as the RON of the hydrocarbon blendstock increases, the temperature for peak OH concentration increases. The relative rates of OH addition and H-abstraction become closer—explaining why higher-RON blendstocks show a less synergistic effect.

Because alcohols, olefins, furans, and prenel have demonstrated synergistic blending [6,18], we chose to investigate ethanol, 2-methyl-2-butene (2M2B), DMF, 2MF, and 3-methyl-2-buten-1-ol (prenol) to represent these four chemical classes. Prenol has functional groups of both an olefin and alcohol. 2M2B was chosen to represent olefins, as it is structurally similar to prenel. Several studies have investigated the mechanism and kinetics of autoignition of ethanol [19,20,21], alkyl-furans [16,22], prenel [23,24,41], and 2M2B [25] in neat form and in some cases as blends with heptane or isooctane. These were blended into the four-component surrogate (as described in Table 1) at blend levels up to nominally 30 vol% for RON measurement. RON was then predicted using kinetic simulations, and the simulations were interrogated to understand which reactions in the model were responsible for RON synergy.

2. Methods

All pure components used in this study were obtained from Sigma Aldrich in > 99% purity. Blends into the four-component surrogate (described in Table 1 above) were prepared by mass and validated by gas chromatography–flame ionization detection (GC-FID). RON was measured in a CFR engine according to ASTM International standard D2699 [4].

The kinetic modeling was performed using the open-source software Cantera [26] and with the 2020 version of the Co-Optimization of Fuels & Engines (Co-Optima) chemical kinetic mechanism, which consists of 4,164 species and 18,732 reactions [27]. Recently, a version of this gasoline kinetic model without the CoOptima blendstocks was published in Cheng et al. [28] The model presented in Cheng et al. [28] contains all BOB components of this work and ethanol. The CoOptima kinetic model of this work is available upon request and a manuscript discussing the model is in development. The CoOptima kinetic model, and any updates, will be hosted on the LLNL combustion website for archival public access. RON was simulated using the chemical kinetics method developed by Westbrook et al. [29]. In this approach, the pressure versus time (or crank angle degree [CAD]) profile from a single-cylinder spark-ignition engine experiment at 600 rpm, equivalence ratio 1.1, and using E30 fuel with RON 104.9 is imposed on a modeled zero-dimensional (0D) reactor simulating the end gas pressure in the engine. For the 0D reactor to follow the experiment pressure curve, the volume of the reactor is varied based on an isentropic process. In this way, the pressure and temperature follow the measured pressure and estimated temperature of the end gas in the engine experiment. The chemical kinetics involved in the simulation release heat as the pressure and temperature increase beyond a certain level. Eventually, the whole mixture autoignites—which is observed as a sharp temperature rise in the model output. We arbitrarily define autoignition as occurring when the temperature reaches 1500 K. The initial pressure and temperature are 3.1 bar and 502 K, respectively, corresponding to the 65.3 CAD before the top dead center in the recorded pressure data. The major assumption of this method is that calculated autoignition times will vary monotonically with RON, allowing the model to be calibrated using fuels of known RON such as the PRF, to produce a curve from which RON can be predicted from the calculated autoignition time. To develop this calibration, we performed simulations for PRF (which define RON values from 0 to 100) and ethane

and methane (with RON to define values of 115 and 130, respectively) to produce autoignition time versus RON curve shown in Fig. 2. While this approach does not consider all of the factors that can affect experimentally measured RON values (such as air–fuel ratio, heat of vaporization, or flame speed), Westbrook’s comparisons of simulation results to experimental measurements show remarkably good agreement consistent with the fact that autoignition chemistry is the primary factor affecting RON [29,30]. The four-component surrogate and its mixtures with the synergistic blendstocks were then simulated to generate an autoignition time, and the curve in Fig. 2 was used to predict RON.

The Gaussian 16 program package [31] was used to calculate Gibbs free energies of OH addition to 2MF. The B3LYP/6-31G(2df,p) level of theory was employed to optimize the structures, and their free energies at room temperature were calculated using the G4 composite method [32]. G4 method was chosen to give the smallest confidence intervals against experimental formation enthalpies and give the closest values of formation enthalpies of radicals compared to the Active Thermochemical Tables (1.48 and 1.08 kcal mol⁻¹, respectively) [33]. To calculate rate parameters, free energies at different temperatures (800 K–1500 K with 20 K intervals) were calculated by running the G4-compatible version of the GoodVibes program [34]. Next, the rate parameters A , n , and E_a were determined by the regression based on equation (2):

$$k_{OH-diss} = k_{OH-add}(RT)^{-1} \exp\left(-\frac{\Delta G}{RT}\right) = AT^n \exp\left(-\frac{E_a}{RT}\right) \quad (2)$$

where $k_{OH-diss}$, k_{OH-add} , and ΔG are reaction rates of OH dissociation, addition, and reaction free energy of OH dissociation. k_{OH-add} was set to 10¹³ cm³ mol⁻¹ s⁻¹ based on the known literature value [35]. Any reference to a rate constant in this work refers to the high-pressure limit unless explicitly stated otherwise. The detailed procedure of rate constant calculations is explained in our previous study [36].

3. Results and discussion

3.1. RON measurements and prediction from kinetic simulation

Measured octane number values for the four-component surrogate and the blendstocks are shown in Table 2. The surrogate was developed to approximate refinery gasoline autoignition properties while providing a simple, well-defined composition for kinetic simulations [6]. The blendstocks were selected as representative of the various classes of compounds that have exhibited synergistic blending – with ethanol, prenel, and the alkyl furans as viable or potentially viable

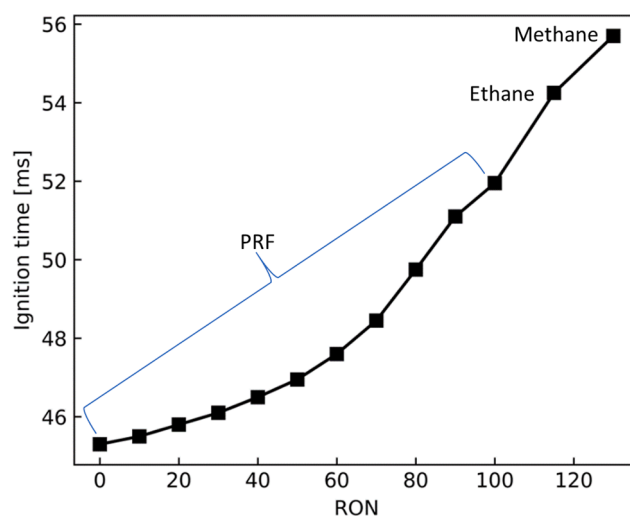


Fig. 2. Calculated autoignition time versus RON model calibration curve based on a range of PRF, ethane, and methane.

Table 2

Octane numbers for blend components were used in this study.

Blendstock	RON	MON	Source
Four-component surrogate	90.3	84.7	[6]
Ethanol	109	90	[37]
3-methyl-2-buten-1-ol (prenol)	93.6	74.2	[38]
2-methyl-2-butene (2M2B)	97.3	84.7	[39]
2-methylfuran (2MF)	102.5	86.1	[39]
2,5-dimethylfuran (DMF)	101.3	88.1	[39]

biofuels based on production pathway and properties [6]. 2M2B is a surrogate for biofuel olefins such as a mixture of diisobutylene isomers and provides a useful comparison to prenol as it has an identical carbon-carbon bond structure but without the hydroxyl group. RON results for blends are shown in Fig. 3. Results for ethanol are repeated from Fig. 1 [6], results for prenol have been published previously [18], and other results are previously unpublished. All blendstocks show synergistic blending at least as significant as that observed for ethanol.

RON predictions using the kinetic simulation approach are also

shown in Fig. 3. The ability to predict RON for single components or blends is a significant test of the accuracy of a kinetic model [29], because simulation covers the temperature range of 500 K to over 2000 K, pressures up to 60 bar, and a change in the predicted ignition delay time (or CAD) of 1 ms changes predicted RON by as much as 10 octane numbers (see Fig. 2). As shown in Fig. 3a, the model provides excellent prediction for the RON of the four-component surrogate (89.3 versus 90.3 measured compared to measurement reproducibility of ± 0.7), as well as for neat ethanol (108.5 versus 109 accepted literature value with a reproducibility of ± 3.5). Predictions for ethanol blends are also in good agreement with the data—in line with the high level of development of the combustion kinetic models for the surrogate components and ethanol. Predicted RON for 2M2B is much less accurate, with the general trend captured up to 40 mol%, above which the model sharply diverges from the data with the predicted RON of neat 2M2B in error by 12 RON units. The predictions for prenol blends do not even capture the experimentally observed synergistic blending effect. The simulations also produce agreement within measurement reproducibility for blends with DMF (Fig. 3e). The predicted RON of DMF itself is high by 2.2 RON units compared to measurement reproducibility of ± 1.4 . Predicted RON

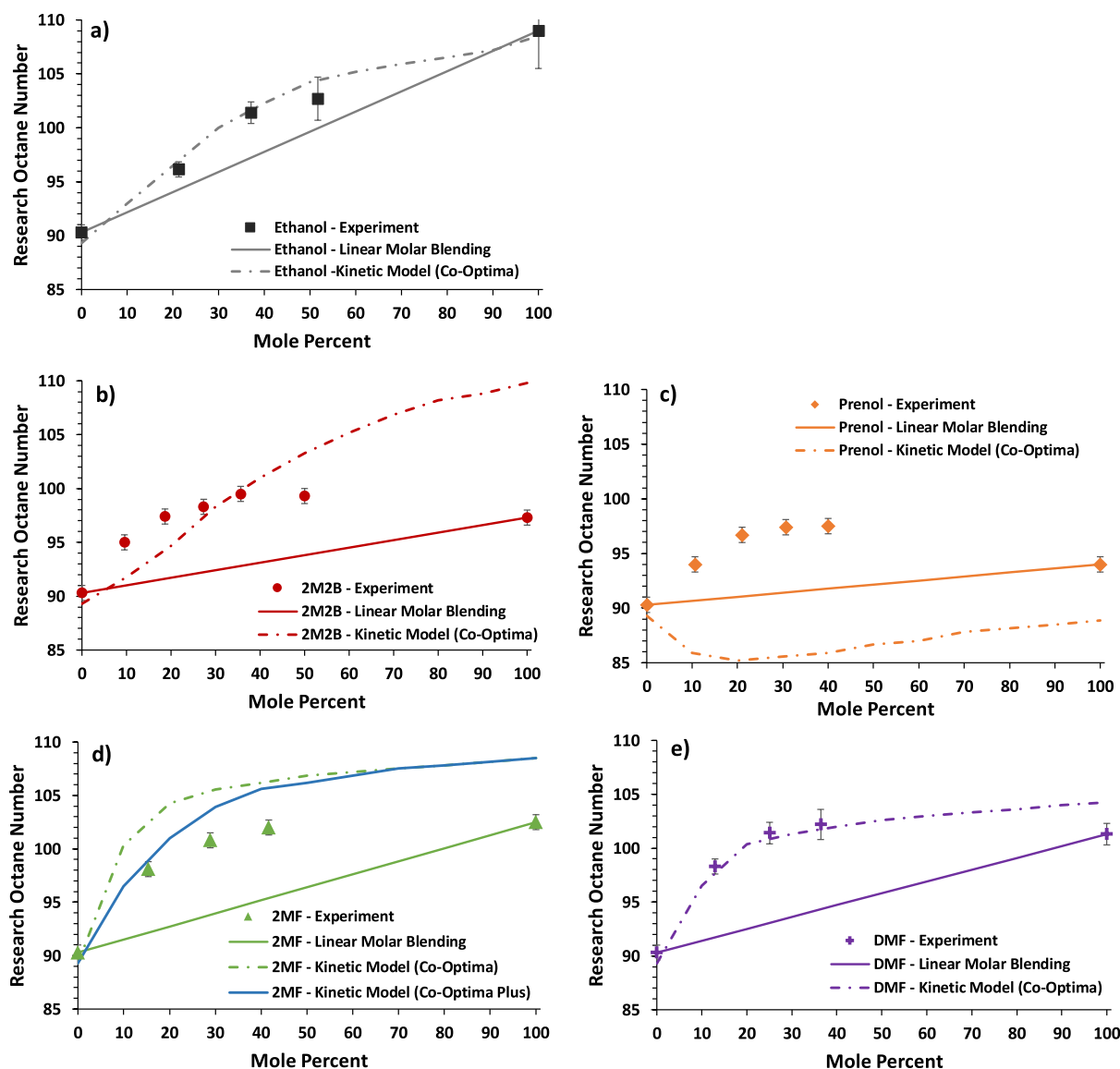


Fig. 3. Measured and predicted RON values for the synergistic blendstocks in the four-component surrogate. In panel (d), Kinetic Model (Co-Optima Plus) includes updated OH addition rates, as discussed later.

values for 2MF blends follow the correct trend but are high by 4 RON units, and the prediction for neat 2MF is high by 6 RON units.

The significant disagreement shown in Fig. 3c warrants a brief discussion of two potential sources of discrepancy that are relevant to comparisons of RON simulations and experiments in this work. First, as noted in section 2, the current modeling approach is incapable of capturing additional influences (such as air-to-fuel ratio, enthalpy of vaporization, or flame speed) that might affect the determination of RON in a CFR engine. It is also worth noting that CFR engines do not measure autoignition timing per se, but measure knock intensity. Knock intensity defined in ASTM D2699 is a measure of the level of abnormal combustion based on analog signals from a detonation pickup. A detonation pickup is a transducer that generates a response proportional to the rate-of-change of cylinder pressure, regardless of autoignition timing. That is, two fuels may have similar knock intensities (i.e. RON) but different autoignition timings. While this work continues to support that autoignition timing and RON (i.e. knock intensity) are often strongly correlated for many neat and blended fuels, that may not be true for every fuel. Significantly more computationally expensive and physics inclusive approaches have been proposed to model CFR engines and knock intensity, including work by Pal et al. [40]. Such approaches are beyond the scope of this work and simulation errors inherent to our current approach cannot be discounted at this time. A second potential source of discrepancy pertains to the accuracy of the kinetic model used. In the case of prenil, it is the subject of relatively new kinetic modeling efforts, experimentally and theoretically relatively understudied, and lacking some combination of accurate reaction pathways, rate constants, and thermodynamic properties. No autoignition data of prenil mixtures, such as with 4-component BOB surrogate fuels, are currently available in the literature to use as validation of the kinetic model for this work. However, the kinetic model for prenil from LLNL was very recently published along with new ignition delay time measurements of neat prenil in Lokachari et al. [41]. The validations provided in Lokachari et al. [41] indicate the model should at a minimum simulate the autoignition of neat prenil well. Quantum chemistry calculations and experimental determinations of rate constants and thermodynamic properties of the relevant species participating in low-temperature

autoignition reactions would benefit all kinetic models discussed in this work. Among the conclusions of Lokachari et al. [41], studies of OH- and HO₂-addition and the subsequent secondary reactions of adducts were recommended to accurately predict the autoignition behavior of prenil. Additional reaction networks recommended by Lokachari et al. [41] for further study include the O₂-addition to resonance stabilized radicals and the oxidation of prenil's stable intermediates, prenil and isoprene.

3.2. Kinetic simulation – Surrogate gasoline

Results extracted from kinetic simulations to predict RON for the four-component surrogate are shown in Fig. 4. Simulated end gas temperature (Fig. 4a) increases from compression until first-stage heat release causes an increase in slope at about -12 CAD, with ignition occurring at 3 CAD. First-stage heat release is observed (Fig. 4b) starting at about 760 K (-15 CAD) in the simulation, peaking at -11.3 CAD. Fig. 4c shows fractional conversion of the fuel components, with approximately 40% of n-heptane, 1-hexene, and isooctane converted to other species in the first-stage reactions. In contrast, toluene is primarily consumed in high-temperature reactions. Simulated radical and H₂O₂ concentrations are shown in Fig. 4d, showing the radicals reaching a local maximum concentration during the first-stage reaction and H₂O₂ concentration increasing to a plateau during first-stage reactions and remaining constant until it decomposes at the time of autoignition.

3.3. Kinetic simulation – Ethanol blends

Kinetic simulations to predict the RON of ethanol/four-component surrogate mixtures along with experimental results are shown in Fig. 3a where agreement between simulation and experiment is within experimental reproducibility. The reactions that consume nearly 94% of ethanol during the first-stage reaction in the simulated RON test are shown in Table 3, and all involve reactions with OH or HO₂ radicals. Ethanol cannot undergo radical addition reactions and can only react via H-atom abstraction reactions, generating radicals primarily on the α carbon (61% ethanol consumed). H-abstraction by HO₂ at the same site

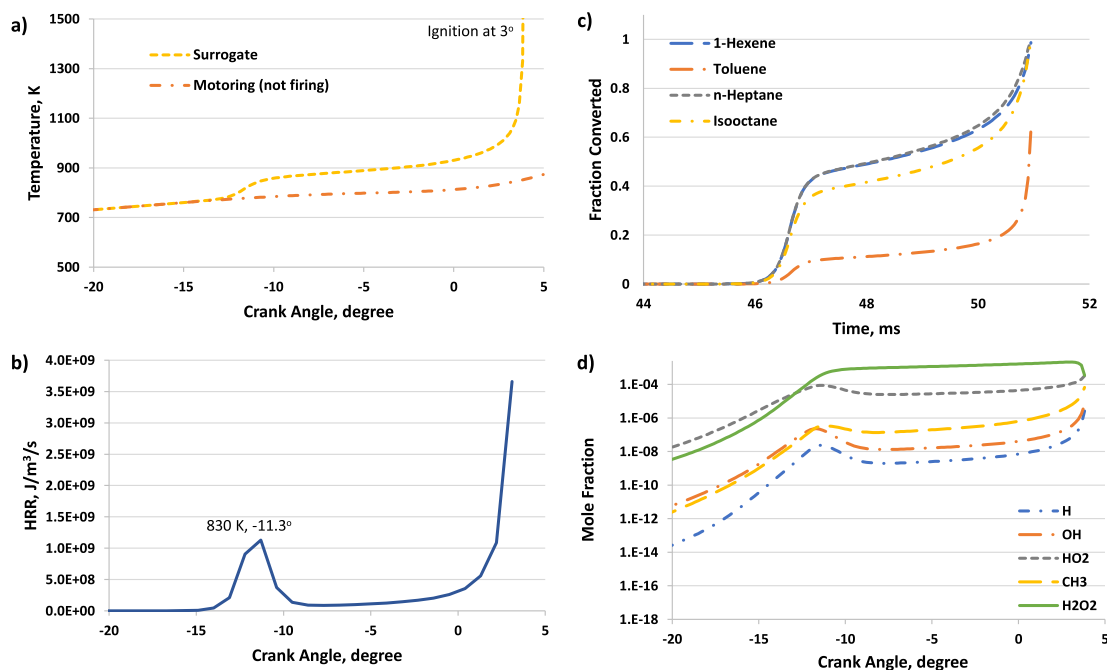


Fig. 4. RON simulation results for the four-component surrogate gasoline: (a) end gas temperature, (b) calculated heat release rate (HRR), (c) fractional conversion of surrogate components, d) mole fraction (log scale) of important species.

Table 3

Top ethanol-consuming reactions during the first-stage reaction (around 800 K) for a 20 mol% blend in the simulated RON test. Reactions consume nearly 94% of ethanol.

Reaction	Net Progress Rate, kmol/m ³ ·s	Product Structure	% Ethanol Consumption
C2H5OH + OH <=> H2O + SC2H4OH	0.108		60.9
C2H5OH + OH <=> H2O + PC2H4OH	0.046		26.1
C2H5OH + HO2 <=> H2O2 + SC2H4OH	0.012		6.6

is a minor reaction (6.6%). A second important reaction consumes OH by H-abstraction at the primary β carbon (26.1%). The α carbon C–H bond is most reactive because it is weakened due to the electron withdrawing strength of the oxygen [11,20]. These reactions consume highly reactive OH and generate less-reactive HO₂ to form other radical species.

As shown in Fig. 5, the α radical reacts with O₂ and proceeds through an elimination reaction to give a less-reactive HO₂ radical and acetaldehyde. The barrier for this reaction is so low that other reaction pathways are unimportant [20,42]. Acetaldehyde is consumed by H-abstraction reactions that result in CO and methyl radical formation and is thus chain propagating [43]. The β radical rapidly reacts to form ethylene and OH radical above 600 K, then reacts with oxygen followed by Waddington reaction to produce formaldehyde and OH, and is thus also chain propagating [44,45]. These reactions are all radical scavenging in the sense that they direct OH into chain propagating pathways and delay it from reacting with n-heptane or isoctane in chain branching pathways.

The effect of this radical scavenging is to reduce the first-stage temperature increase relative to the surrogate without ethanol (Fig. 6a) and reduce and delay first-stage heat release (Fig. 6b) from –11 to –8 CAD. At the end of the first stage, the conversion of fuel hydrocarbon components has been reduced by about one-third for the ethanol blend relative to the surrogate without ethanol. Peak OH concentration (Fig. 6d) during the first-stage reaction is also significantly reduced. This, in turn, delays the crank angle (or ignition delay time), where the decomposition of H₂O₂ initiates high-temperature autoignition. At just after 0 CAD, near the onset of high-temperature autoignition, only about 20% to 30% of the ethanol has been consumed, and ethanol is being consumed in the same or similar reactions with radicals that lead to chain propagation rather than chain branching (see Fig. S1 and Table S-1 in Supplemental Material). These combined factors lead to the observed synergistic RON blending. The overall mixture is less reactive than predicted by simple dilution of the surrogate with ethanol (as assumed by a linear molar blending model).

3.4. Kinetic simulations – Dimethylfuran and 2-Methylfuran

DMF was the most effective synergistic blending component of those

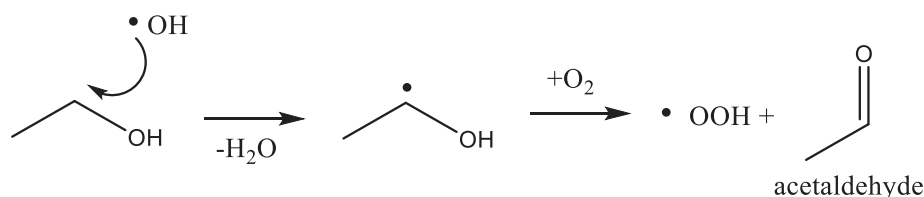


Fig. 5. Reaction pathway for ethanol showing H atom abstraction followed by reaction of the resulting radical with molecular O₂ and formation of acetaldehyde.

investigated, with 2MF second-most effective (in terms of ON_{imb} or total octane number increase from interactions between the blendstock and the hydrocarbon fuel as discussed below). Fig. 3d and Fig. 3e show simulated and experimental RON values for DMF and 2MF. Notably, for DMF, the pure component DMF RON value of 101.3 is achieved at the 25 mol% blending level, whereas for 2MF, the pure component value of 102.5 is achieved at the highest blend level 42 mol%. The kinetic simulations produce blend RON values for DMF blends that are within experimental reproducibility of measured values. The simulation overpredicts neat DMF RON by 2.2 RON units with experimental uncertainty of ± 1.4 units. For 2MF, the simulation overpredicts blend RON by 4 units and neat 2MF RON by 6.

DMF and 2MF present two possible reaction pathways involving the addition of OH radical to the ring or H-abstraction from the alkyl group via OH radical. These are the top two reactions consuming DMF during the first-stage ignition based on the kinetic simulation as indicated in Table 4, with 81% consumed by OH addition at the 2 or 5 carbons and 14.5% consumed by H-abstraction from a methyl group. For 2MF, OH addition at the 2 or 5 carbons produces different intermediates, accounting for 82% of 2MF consumption, whereas H-abstraction accounts for 14% (Table 5).

Fig. 7 shows these reaction pathways and subsequent reactions of the products based on the published mechanisms that are the basis of the mechanism used here [16,46]. After OH radical adds to the furan ring, a rapid ring-opening reaction occurs due to the weakened C–O ether bond in the ring, leading to a radical similar to diacetyl ethylene (3-hexene-2,5-dione) from DMF and 4-oxo-2-pentenal from 2MF. The ring-opening products decompose to methyl vinyl ketone, acetyl radical (from DMF), and formyl radical (from 2MF) and are therefore chain propagating. The H-abstraction products (resonance-stabilized radicals, RSR) from DMF and 2MF can react with HO₂ or other radical species, ultimately forming 5-methylfurfural (for DMF) or furfural (for 2MF) and an OH radical and are therefore also chain propagating. For alkyl radicals one might also expect RO₂ pathways to be important. However, the resonance nature of the radicals generated from 2MF and DMF leads to shallower RO₂ wells with no fast RO₂-isomerization or HO₂-elimination reactions readily available. While RSR + HO₂ reactions are considered in the current kinetic model for 2MF and DMF, RSR-RSR association reactions are not. The presence of RSR-RSR association reactions are generally expected to inhibit reactivity at low temperatures, thus leading to higher RON predictions if they were added to the current kinetic model.

This radical scavenging reduces and delays the first-stage temperature increase (Fig. 8a) and reduces and delays heat release rate (Fig. 8b). At 20 mol% DMF, the first-stage autoignition appears to have been eliminated completely along with its accompanying heat release. At 20 mol%, DMF delays the onset of high-temperature autoignition by 0.4 ms relative to ethanol, resulting in a RON that is 4 units higher. Recent research has shown that DMF can also increase intermediate temperature heat release around 900 K, leading to high sensitivity of ignition delay to the fuel–air ratio (ϕ -sensitivity) [47], and we also see higher heat release at 900 K for the 5% and 20% DMF blends (See Fig. S3 in Supplemental Material). Like the case for ethanol, at a few degrees past 0 CAD, near the onset of high-temperature autoignition, only about 20% of the DMF has been consumed for the 20 mol% cases (see Fig. S4 in Supplemental Material). Where the decomposition of H₂O₂ initiates

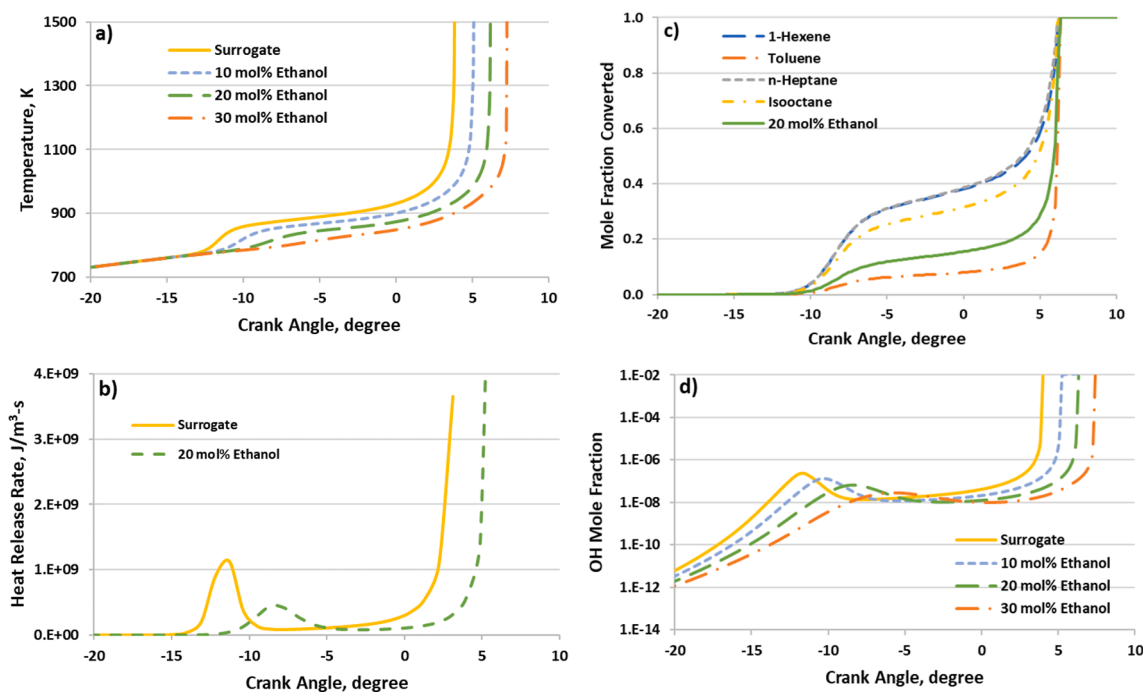


Fig. 6. (a) Temperature rise, (b) heat release rate, (c) reactant conversion for 20 mol% ethanol, and (d) OH radical concentrations for simulation of RON for ethanol blends.

Table 4

Top DMF-consuming reactions during first-stage heat release (around 800 K) for a 5 mol% blend in the simulated RON test. Reactions consume over 95% of DMF.

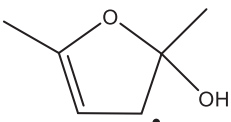
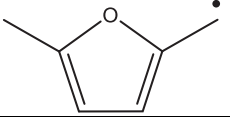
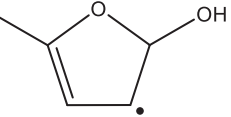
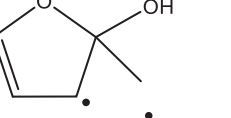
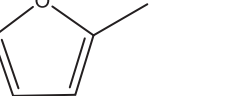
Reaction	Net Progress Rate, $\text{kmol}/\text{m}^3\cdot\text{s}$	Product Structure	% DMF Consumption
DMF25 + OH \rightleftharpoons DMF252OH3J	0.092		81.4
DMF25 + OH \rightleftharpoons DMF252J + H ₂ O	0.017		14.5

Table 5

Top 2MF-consuming reactions during first-stage heat release (around 800 K) for a 5 mol% blend in the simulated RON test. Reactions consume over 95% of 2MF.

Reaction	Net Progress Rate, $\text{kmol}/\text{m}^3\cdot\text{s}$	Product Structure	% 2MF Consumption
MF2 + OH \rightleftharpoons MF25OH4J	0.060		42
MF2 + OH \rightleftharpoons MF22OH3J	0.058		40.6
MF2 + OH \rightleftharpoons H ₂ O + MF22J	0.020		14

high-temperature autoignition, DMF is being consumed in the same or similar reactions with radicals that lead to chain propagating rather than chain branching products.

4. Discussion

In the simplest terms, the mechanism of synergistic blending is scavenging of OH radicals produced by the low-temperature autoignition reactions of the most reactive components of the BOB (e.g., paraffins) by the added blendstock. Radical scavengers are compounds that react with initial OH radicals that then produce less-reactive radicals or products. As radical-scavenging compounds are blended into gasoline, these blendstocks compete for OH radicals, removing them from the radical pool before they can react with more reactive components in gasoline, reducing the overall reactivity of the system and shutting down low-temperature autoignition. This is observed in these simulations as shutting down first-stage reaction and heat release. This shifts the transition to high-temperature autoignition—above 900 K, where H₂O₂ decomposition occurs—to later in time or higher CAD in the simulated RON test or requires a higher compression ratio at constant end-gas autoignition timing in the physical RON test. The effect of radical scavengers is caused by interaction between them and the reacting components of the gasoline. As described in the Introduction, Anderson et al. [7] proposed the parameter ON_{int} , or the RON increase from interactions between the blendstock and the hydrocarbon fuel (i.e., the difference between the measured RON and predicted from a linear molar blending model). Fig. 9 shows ON_{int} for the blendstocks examined here. DMF provides the most significant degree of interaction, with 2MF, 2M2B, and prenil at an intermediate level, followed by ethanol at a significantly lower level. As potential future biofuels, the alkyl furans and prenil would allow higher finished blend RON using today's refinery blendstocks, or the lowering of the refinery blendstock RON to achieve today's RON levels (potentially at reduced refinery blendstock cost).

It is noted that reaction mechanisms for ethanol, DMF, and to a lesser extent 2MF were able to predict RON for blends with the surrogate, or in the case of 2MF, to predict the RON trend. Therefore, the important

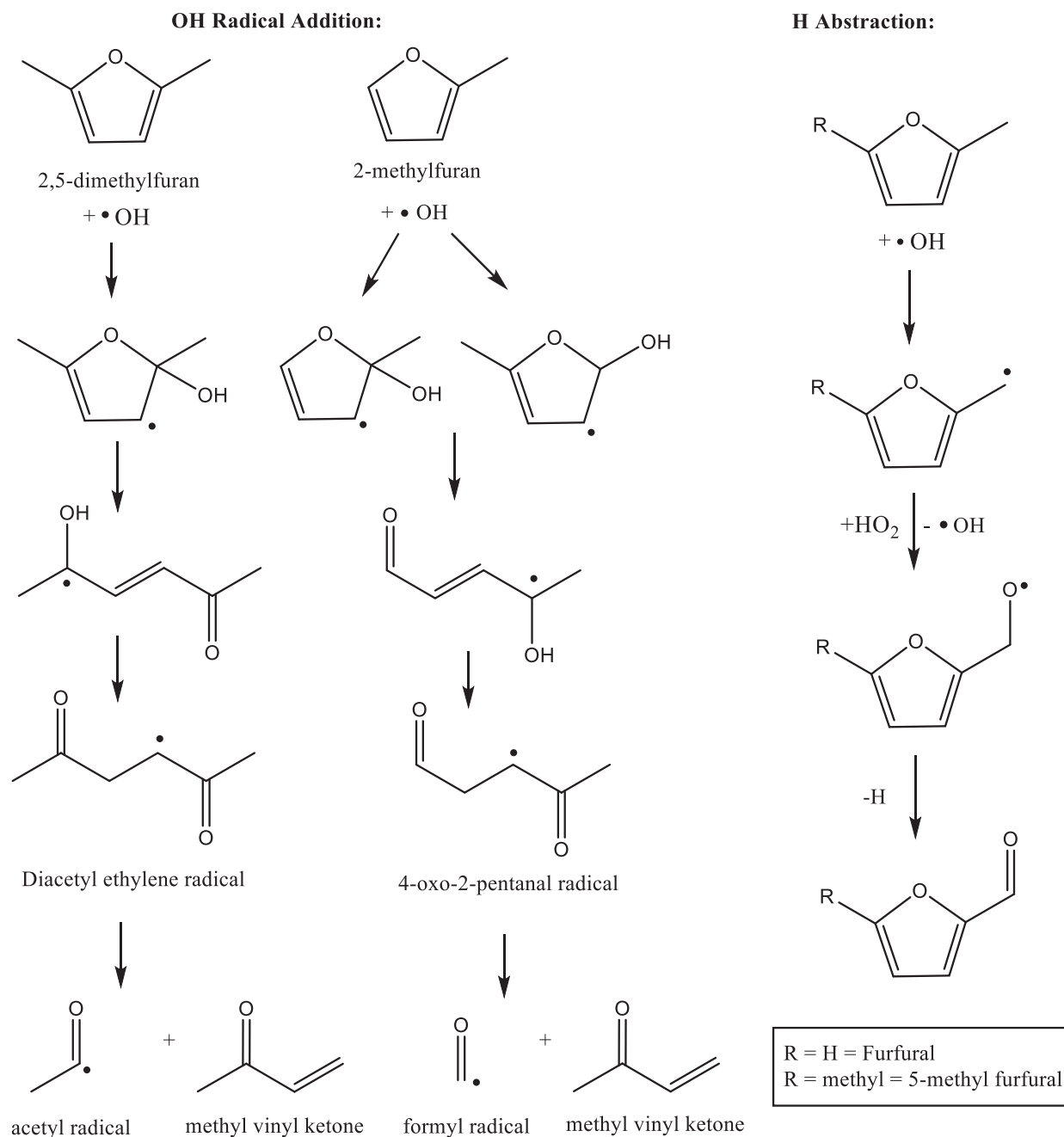


Fig. 7. Reaction pathways for 2MF and DMF.

reactions for radical scavenging for these blendstocks are discussed below. For 2M2B and prenol, the kinetic mechanisms are not yet at a point in their development that they can shed light on the source of their synergistic blending effect, although they have a double bond that can undergo OH addition reactions which are important. Further development of these models is warranted and is underway for 2M2B, some aspects of this are also discussed below.

Table 6 shows reactions in the simulation accounting for over 90% of conversion for each component at the peak of the first-stage heat release for the surrogate gasoline, as well as blends of the surrogate with 5 mol% DMF and 20 mol% ethanol (5 mol% DMF is used because at 20 mol% DMF, the first-stage reaction was eliminated). Additional reactions are shown in Table S-3 of the Supplemental Material. Net progress rate (NPR) is defined as the net forward reaction minus the net reverse reaction. NPRs are much higher for isooctane because it is present at the

highest concentration in the surrogate. Notably, all these reactions for isooctane, n-heptane, and toluene are H-abstractions leading to the formation of water (or HO₂) and radicals, whereas, for 1-hexene, there are also OH and H-addition reactions to the double bond. As DMF and ethanol are blended in, the NPRs of H abstraction by OH of the surrogate components are reduced, as OH instead reacts with the blendstock and is scavenged from the radical pool. The rates of consumption of the surrogate components are dramatically reduced (the sum of all NPRs is reduced for the DMF and ethanol blends). For example, DMF at only 5 mol% reduces the NPR for H-abstraction reactions from the surrogate components by >40%, whereas 20 mol% ethanol reduces these reactions by 56%. For DMF, OH addition to the ring has the highest NPR, and for ethanol, H abstraction at the α carbon has the highest NPR. As these are the most significant reactions identified in the simulations, our discussion will focus on these key pathways.

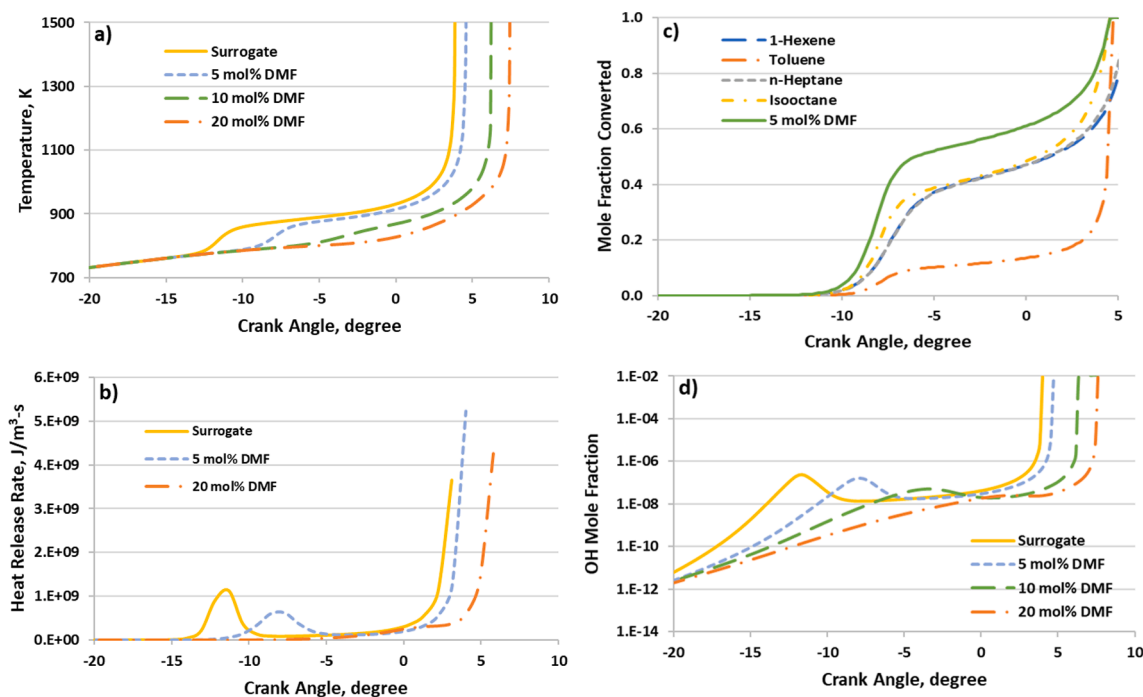


Fig. 8. (a) Temperature rise, (b) heat release rate, (c) reactant conversion for 5 mol% DMF, and (d) OH radical concentrations for simulation of RON for DMF blends.

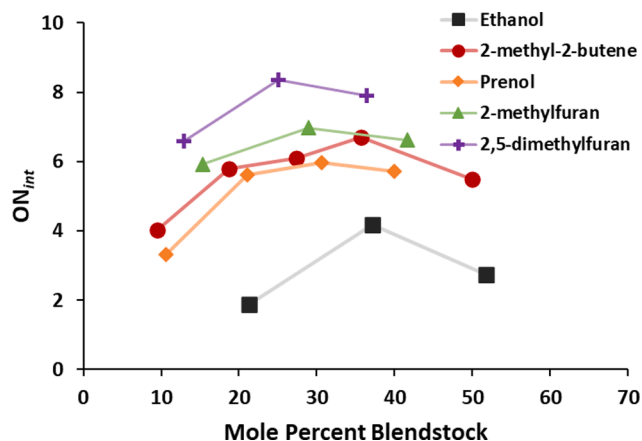


Fig. 9. ON_{int} (the RON increase from interactions between the blendstock and the hydrocarbon fuel) versus mole fraction blended for the RON experiments reported in Fig. 3.

Fig. 10 shows the total rate constant for OH consumption as a function of temperature for reactions with the blendstocks considered here. It is interesting to examine the rate constants at about 800 K to 850 K because Mehl et al. [48] found that 825 K correlates well with the anti-knock index $([RON + MON]/2)$, and our simulations of RON showed the peak first-stage heat release in this range. Note that the uncertainty in the rate constants for OH with ethanol at 800 K–850 K is about $\pm 20\%$ [49]. For DMF, the abstraction rate has an uncertainty of $\pm 50\%$ [33], and the addition rate constant has an uncertainty of a factor of three [22]. For prenil and 2M2B, the uncertainty factors are estimated to be two for abstraction and a factor of 2–10 for addition, depending on the site. As seen in Fig. 10 at 850 K, DMF has the highest reaction rate with OH of the blendstocks being considered, and ethanol has the lowest rate. Prenol and 2M2B fall into the middle region. The rates for 2M2B are from the Co-Optima mechanism and are based on rates for propene [50]. Rates for prenil were recently calculated [51]. Note that 2MF is not plotted because kinetic models assume the same OH addition and H-

Table 6

Primary reactions consuming surrogate gasoline components and blendstocks at the peak of first-stage heat release, accounting for 90% of species conversion.

	0% blend	5% DMF	20% ethanol
CAD/temperature (K) at peak of first-stage heat release	-11.3/830	-8/824	-8.6/807
Isooctane	NPR (kmol/m ³ ·s)	NPR (kmol/m ³ ·s)	NPR (kmol/m ³ ·s)
IC8 + OH \rightleftharpoons H2O + IC8-radical	1.59	0.95	0.71
n-Heptane			
NC7H16 + OH \rightleftharpoons H2O + C7H15-radical	0.56	0.35	0.26
Toluene			
C6H5CH3 + OH \rightleftharpoons C6H5CH2 + H2O	0.27	0.14	0.10
C6H5CH3 + OH \rightleftharpoons C6H4CH3 + H2O	0.076	0.038	0.027
C6H5CH3 + O2 \rightleftharpoons C6H5CH2 + HO2	-0.037	-0.017	-0.012
1-Hexene			
C6H12-1 + OH \rightleftharpoons H2O + C6H11-radical	0.069	0.043	0.032
C6H12-1 + OH \rightleftharpoons C6H12OH	0.052	0.035	0.027
C6H12-1 + H \rightleftharpoons C6H13-2	0.021	0.012	0.0063
DMF			
DMF25 + OH \rightleftharpoons DMF25OH3J	N/A	0.127	N/A
DMF25 + OH \rightleftharpoons DMF252J + H2O	N/A	0.027	N/A
DMF25 + H \rightleftharpoons H4E2O3J	N/A	0.007	N/A
Ethanol			
C2H5OH + OH \rightleftharpoons H2O + SC2H4OH	N/A	N/A	0.11
C2H5OH + OH \rightleftharpoons H2O + PC2H4OH	N/A	N/A	0.046
C2H5OH + HO2 \rightleftharpoons H2O2 + SC2H4OH	N/A	N/A	0.012
C2H5OH + OH \rightleftharpoons C2H5O + H2O	N/A	N/A	0.005

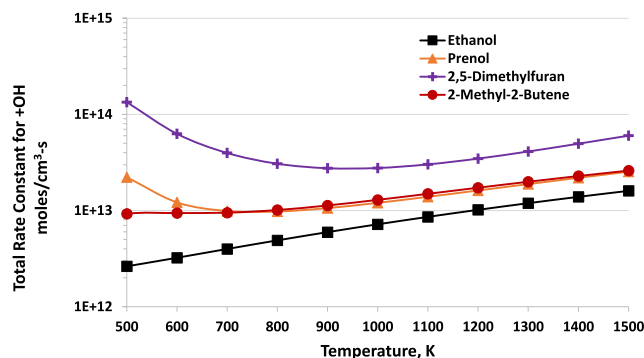


Fig. 10. Total rate constant for OH consumption by reaction with blendstocks versus temperature for ethanol [52], prenol [51], 2M2B [27], and DMF [53].

abstraction rates as used for DMF [16]. This total rate constant behavior correlates with the behavior seen in Fig. 9, in which DMF has the highest ON_{int} and ethanol has the lowest at the blending levels tested, confirming the concept that OH radical scavenging is the most important reaction for RON synergy.

One key difference between ethanol and the other blendstocks investigated is that ethanol reacts with OH in H-abstraction reactions only, whereas the other blendstocks can also undergo OH addition reactions. A recent review article by Rotavera and Taatjes [54], highlights and discusses the variation of branching ratios that can be found in literature for ethanol + OH. In this work the rate constants of Sivaramakrishnan et al. [55] are utilized. These rate constants result in a beta site selectivity that is the lowest of the three discussed in Rotavera and Taatjes [54]. Site selectivity will play a role in the competition between OH (from the beta site) or HO₂ (from the alpha site) chain-propagating pathways resulting from ethanol. However, the overall rate constants of ethanol + OH are in good agreement across the studies cited by Rotavera and Taatjes [54]. That is the selectivities do not significantly change the overall degree to which ethanol consumes OH relative to other fuel components. Either ethanol site, alpha or beta, ultimately propagates radicals (OH from the beta site and HO₂ from the alpha) where the n- and iso-alkane components of the BOB are the primary sources of OH-radical chain branching through conventional low temperature chemistry pathways. Fig. 11 shows branching ratios for OH addition and H-abstraction for prenol, 2M2B, and DMF. According to these calculated rate constants, H-abstraction becomes dominant for prenol and 2M2B at 600 K to 750 K, whereas OH addition remains dominant for DMF up to nearly 1200 K. In addition to a faster rate of reaction with OH, DMF exhibits higher ON_{int} because of the persistence of OH addition as the dominant reaction through the entire first-stage autoignition temperature range.

A review of the reaction rates for OH abstraction and DMF reveals that rates calculated using G3 are available. H-abstraction rate constant is $k = 1.016 \times 10^4 T^{3.133} \exp(-1085/T) \text{ cm}^3/\text{mol}\cdot\text{s}$ [53]. The OH addition rate constant is $k = 2.21 \times 10^4 T^{2.45} \exp(+3649/T) \text{ cm}^3/\text{mol}\cdot\text{s}$; note the negative activation energy [22]. The Co-Optima mechanism incorporates these rates for DMF. For 2MF, the mechanism uses a previously proposed model that assumes OH addition rates to the 2 and 5 carbons are identical and that they were the same as for DMF [16]. The OH addition to alkylfurans has also been studied in atmospheric chemistry. In early work, Bierbach et al. [56] found that (at 300 K) OH addition rates depended on the number of methyl groups on the furan ring, with higher rates for more methyl groups. Their experimentally measured OH addition rates for DMF were approximately twice those for 2MF. Aschmann et al. [57] used a different methodology in a more recent study but came to the same conclusion. This atmospheric chemistry-focused work also finds rapid ring opening and the formation of diacetyl ethylene from DMF. Most recently, Whelan et al. [58] took new low temperature OH-Laser Induced Fluorescence measurements for

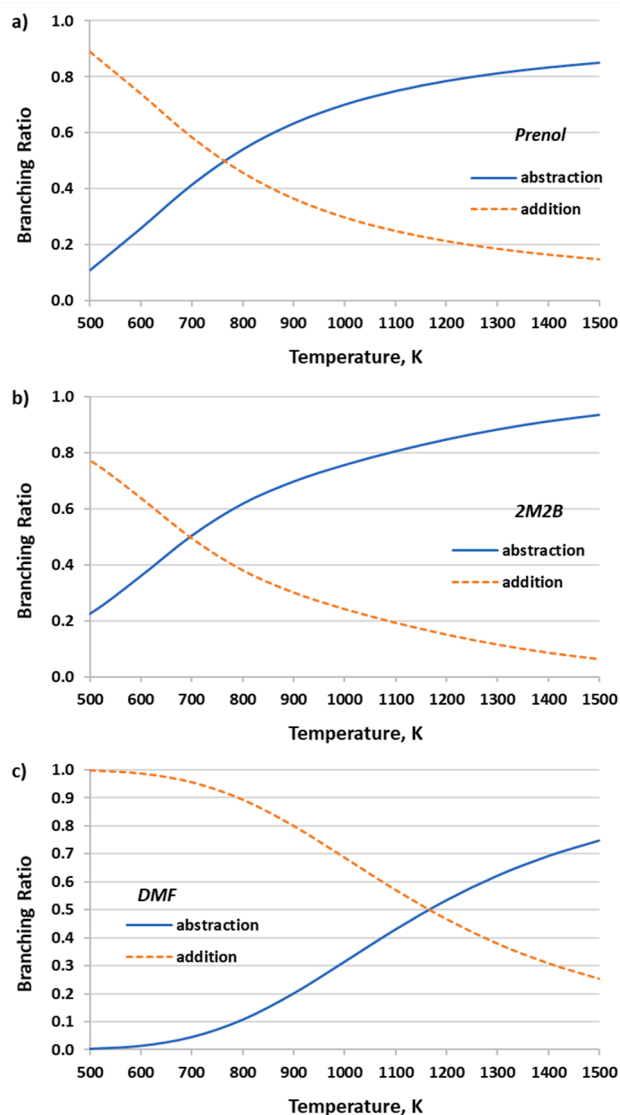


Fig. 11. Branching ratios for OH addition ($k_{add}/(k_{add} + k_{abs})$) and H-abstraction ($k_{abs}/(k_{add} + k_{abs})$) for (a) prenol [51], (b) 2M2B [27], and (c) DMF [53].

furan, 2-methylfuran, and 2,5-dimethylfuran to fit pseudo-first order rate constants. Combining their results with additional literature studies, Whelan et al. [58] conducted a master equation analysis with Master Equation Solver for Multi Energy well Reactions (MESMER) to fit overall rate constants suitable for high and low temperatures. Whelan et al. [58] found the OH-addition (and OH-abstraction) rate constants to be ordered such that $k_{DMF} > k_{2MF} > k_F$ at all temperatures considered. Whelan et al. [58] explain this rate constant trend at low temperatures by noting the increased stabilization of the OH-furan adduct with increased substitution of the furan ring. High quality variational and multi-reference based theoretical calculations would be beneficial to provide additional depth to, and confirmation of, the studies discussed here.

As these rates are the rates used in the Co-Optima model, the use of the DMF rates for OH addition to 2MF overestimates the ability of 2MF to scavenge OH relative to DMF. It is potentially responsible for the poor agreement between RON data and simulations. To modify the 2MF model, the rate constant of OH addition to both carbon 2 and 5 was assumed to be $k = 1.0 \times 10^{13}$ based on a prior study [59]. This value is lower than the OH addition rates for DMF at any temperature, but markedly lower at low temperatures. The rate constant of the reverse reaction (i.e., OH dissociation) was calculated as described in Section 2.

Rate constants were found to be $k = (5.15 \times 10^{14}) \times \exp(-15894/T)$ for OH addition to carbon 2 and $(4.95 \times 10^{14}) \times \exp(-16375/T)$ for OH addition to carbon 5. RON predictions using this updated model (Co-Optima Mechanism Plus) are shown in Fig. 2d. The prediction of RON is significantly improved up to about 30 mol% blend level but did not change the model predictions above about 50 mol%. The first-stage heat release, where these OH reactions play a key role, is eliminated at high 2MF blend levels, which may account for the minimal impact of changing the rates and points to some other issue with the 2MF model at temperatures above 900 K.

The product species formed from these OH reactions must also be considered. These products may further react in chain terminating, chain propagating, or chain branching reactions. Each of the blendstocks investigated in this paper has various mechanisms for OH radical scavenging that are unique. For ethanol, the main pathway by which OH radicals are scavenged is H-abstraction at the α carbon, with H-abstraction by OH consuming nearly 60% of ethanol reacting during the first-stage reaction (Table 3) eventually leading to acetaldehyde and an HO₂ radical that is less reactive at low temperatures. Also, OH can abstract an H from the β carbon in a chain propagating step, producing ethylene and OH. Acetaldehyde and ethylene are also formed in the combustion of the surrogate hydrocarbon components. In the RON test simulation, concentrations of these ethanol reaction products are lower up to about -17 CAD when ethanol is blended into the gasoline surrogate (see Fig. S2 in Supplementary Material). However, the maximum acetaldehyde concentration, a species primarily derived from ethanol, increases with ethanol blending fraction. Ethylene likely decreases with ethanol blending fraction because the reactions leading to its formation from the hydrocarbon species, such as n-heptane, are reduced by ethanol's radical scavenging effect.

Although the kinetic mechanisms for preno1 and 2M2B could not successfully predict RON, the primary OH scavenging reactions above 800 K will be H-abstractions. This seems consistent with De Bruycker et al. [23] for preno1 and Westbrook et al. [25] for 2M2B. The radicals formed are resonance-stabilized allylic radicals and resist unimolecular decomposition below a critical temperature of about 900 K. At low temperatures, these allylic isopentyls or hydroxy pentyl radicals react steadily with molecular oxygen to produce isoprene and HO₂ radicals (or similar species from preno1) that are less reactive at low temperatures. In reviewing the RON simulations for these blendstocks at 20 mol %, preno1 had almost no effect on simulated OH concentration or timing (e.g., CAD at peak reaction) during the first-stage reaction and only slightly reduced first-stage heat release (Fig. S5 Supplementary Material). Updating the reaction rates of OH addition to preno1 and the reactions of the adduct formed with more accurate quantum chemistry calculations may solve the issue of preno1 having almost no effect on the simulated OH concentration during the first-stage reaction and heat release. In 2M2B, the simulations show 20 mol% 2M2B to slightly reduce first-stage OH concentration and heat release and shift peak OH and heat release by almost 5 CAD. Updating the rate constants for abstraction and addition by OH with more accurate quantum chemistry calculations may lead to an improved ability to simulate RON, given the high importance of reactions with OH.

For the alkylfurans, in contrast to ethanol, kinetic simulations show that OH addition pathways are the dominant reactions for removing OH radicals. Hydroxyl addition to the furan ring has a very low or negative activation energy barrier based on quantum mechanics-based rate calculations [22]. The initial resonance-stabilized OH addition products undergo a rapid ring opening (isomerization) due to the weak C-O bond on the ring. The concentration of the initial addition product remains near zero, which drives the equilibrium of the OH addition reaction forward. This contrasts with preno1 and 2M2B, where the OH addition product can more easily react back to the fuel molecule and OH radical through the reverse reaction. Given the importance of the OH addition product ring opening, additional research on the rate of this reaction and the fate of the reaction products seems justified. In the current model,

ring-opening products react to form acetyl (from DMF) or formyl (from 2MF) radicals and stable products such as methyl vinyl ketone from DMF (Fig. 7). Additional mole fraction of key species versus crank angle degrees for 20 mol% DMF in surrogate is shown in the Supplemental Material Fig. S6.

The high ON_{int} of DMF and 2MF is thus caused by their rapid reactions to add OH and the strong thermodynamic driving force caused by rapid subsequent reaction of the OH addition product and the following reaction products, which do not produce much chain branching.

5. Conclusions

Kinetic simulations of various synergistic blending components predicted blending RON well for DMF and ethanol in a four-component surrogate, with predictions of the blends within the reproducibility of the ASTM test. The predictions were not as accurate for 2MF (off by 4 RON units for blends and 6 RON units for the pure component) and 2M2B where the model sharply diverges above the 40% blend level and is in error by 12 RON units for the pure component. For preno1, the model does not capture the synergistic blending behavior observed experimentally. For 2MF, OH radical addition rates to the 2 and 5 position on the furan ring are the same as for OH addition to DMF. Updating these rates resulted in better agreement up to 30 mol% blends (up to about 100 RON). Additional model improvement is needed to predict RON at higher blend levels where the first-stage autoignition has been eliminated. Based on the poor predictions for 2M2B and preno1, further development of these models is necessary and will be the subject of future endeavors.

Interrogation of the kinetic mechanism showed that there was a strong first-stage reaction peaking at about 800 K. Synergistic blendstocks consumed OH radicals during the first-stage reaction for the gasoline surrogate without blendstock. In the RON simulations, this delayed and reduced both the intensity of the first-stage heat release and the first-stage temperature rise. This, in turn, shifted the onset of high-temperature (900 K) autoignition reactions involving H₂O₂ decomposition to later in time or higher CAD or would require a higher compression ratio at constant end gas autoignition timing in the physical RON test. This is responsible for the nonlinear effect of these blendstocks on RON.

The different capability of the blendstocks to scavenge OH radicals away from the reactive components of the surrogate allows them to be ranked in their RON boosting ability. It was noted that good synergistic blenders exhibit more OH addition rather than H-abstraction reactions. In addition, 2M2B and preno1—which can form resonance-stabilized radical products—lead to superior RON boosting compared to ethanol. DMF and 2MF were shown to have the highest RON boosting ability due to the rapid reaction of the OH addition products to other species that pull the OH addition equilibrium toward products.

CRedit authorship contribution statement

Gina M. Fioroni: Conceptualization, Investigation, Writing - original draft. **Mohammad J. Rahimi:** Methodology, Software, Writing - original draft. **Charles K. Westbrook:** Validation, Writing - review & editing. **Scott W. Wagnon:** Formal analysis, Writing - review & editing. **William J. Pitz:** Validation, Writing - review & editing. **Seonah Kim:** Formal analysis, Writing - review & editing. **Robert L. McCormick:** Conceptualization, Supervision, Writing - original draft.

Declaration of Competing Interest

The authors declare that they have no known competing financial interests or personal relationships that could have appeared to influence the work reported in this paper.

Acknowledgements

This research was conducted as part of the Co-Optimization of Fuels & Engines (Co-Optima) project sponsored by the U.S. Department of Energy's Office of Energy Efficiency and Renewable Energy Bioenergy Technologies Office and Vehicle Technologies Office. Co-Optima is a collaborative project of several national laboratories initiated to simultaneously accelerate the introduction of affordable, scalable, and sustainable biofuels and high-efficiency, low-emission vehicle engines. Work at the National Renewable Energy Laboratory was performed under Contract No. DE-347AC36-99GO10337. Work at Lawrence Livermore National Laboratory was performed under Contract DE-AC52-07NA27344. The U.S. Government retains and the publisher, by accepting the article for publication, acknowledges that the U.S. Government retains a nonexclusive, paid-up, irrevocable, worldwide license to publish or reproduce the published form of this work, or allow others to do so, for U.S. Government purposes. Computer time for DFT calculations was provided by the Extreme Science and Engineering Discovery Environment (XSEDE) which is supported by National Foundation grant number TG-CHE200128. The authors acknowledge Dr. Goutham Kukkadapu for assistance in supplying rate constants and for advice on data interpretation, and Dr. Yeonjoon Kim for assistance in calculation of 2MF OH addition rates.

Appendix A. Supplementary data

Supplementary data to this article can be found online at <https://doi.org/10.1016/j.fuel.2021.121865>.

References

- Leone T, Anderson J, Davis R, Iqbal A, Reese R, Shelby M, et al. The Effect of Compression Ratio, Fuel Octane Rating, and Ethanol Content on Spark-Ignition Engine Efficiency. *Environ Sci Technol* 2015;49:10778–89.
- Splitter D, Pawlowski A, Wagner R. A historical analysis of the co-evolution of gasoline octane number and spark-ignition engines. *Front Mech Eng* 2016;1:16.
- Szybist J, Busch S, McCormick R, Pihl J, Splitter D, Ratcliff M, et al. What fuel properties enable higher thermal efficiency in spark-ignited engines? *Prog Energy Combust Sci* 2020;82:100876.
- ASTM International. ASTM D2699–16e1. Standard Test Method for Research Octane Number of Spark-Ignition Engine Fuel. West Conshohocken, PA: ASTM International; 2016.
- Anderson JE, DiCiccio DM, Ginder JM, Kramer U, Leone TG, Raney-Pablo HE, et al. High octane number ethanol–gasoline blends: Quantifying the potential benefits in the United States. *Fuel* 2012;97:585–94.
- McCormick R, Fioroni G, Fouts L, Christensen E, Yanowitz J, Polikarpov E, Albrecht K, Gaspar D, Gladden J, George A. Selection Criteria and Screening of Potential Biomass-Derived Streams as Fuel Blendstocks for Advanced Spark-Ignition Engines. *SAE Int J Fuels Lubr* 2017;10(2).
- Anderson J, Leone T, Shelby MWT, Bizub J, Foster M, Lynskey M, Polovina D. Octane Numbers of Ethanol-Gasoline Blends: Measurements and Novel Estimation Method from Molar Composition. *SAE Technical Paper No. 2012-01-1274*. 2012.
- Badra J, AlRamadan AS, Sarathy SM. Optimization of the octane response of gasoline/ethanol blends. *Appl Energy* 2017;203:778–93.
- Foong TM, Morganti KJ, Brear MJ, da Silva G, Yang Yi, Dryer FL. The Octane Numbers of Ethanol Blended with Gasoline and its Surrogates. *Fuel* 2014;115:727–39.
- Anderson J, Wallington T. Novel Method to Estimate the Octane Ratings of Ethanol-Gasoline Mixtures Using Base Fuel Properties. *Energy Fuels* 2020;34:4632–42.
- Haas F, Chaos M, Dryer F. Low and intermediate temperature oxidation of ethanol and ethanol-PRF blends: An experimental and modeling study. *Combustion and Flame* 2009;156:2346–50.
- Singh E, Tingas E-A, Goussis DIH, Sarathy S. Chemical Ignition Characteristics of Ethanol Blending with Primary Reference Fuels. *Energy Fuels* 2019;33:10185–96.
- Alleman T, Singh A, Christensen E, Fouts L, Simmons E, Johnston G, et al. Octane Modeling of Isobutanol Blending into Gasoline. *Energy Fuels* 2020;34(7):8424–31.
- Christensen E, Yanowitz J, Ratcliff M, McCormick R. Renewable Oxygenate Blending Effects on Gasoline Properties. *Energy Fuels* 2011;25:4723–33.
- Singh E, Shankar VSB, Tripathi R, Pitsch H, Sarathy SM. 2-Methylfuran: A bio-derived octane booster for spark-ignition engines. *Fuel* 2018;225:349–57.
- Tripathi R, Burke U, Ramalingam AK, Lee C, Davis AC, Cai L, et al. Oxidation of 2-methylfuran and 2-methylfuran/n-heptane blends: An experimental and modeling study. *Combust Flame* 2018;196:54–70.
- Shankar V, Li Y, Singh E, Sarathy M. Understanding the synergistic blending octane behavior of 2-methylfuran. *Proc Combust Inst* 2020.
- Monroe E, Gladden J, Albrecht K, Bays J, McCormick R, Davis R, et al. Discovery of novel octane hyperboosting phenomenon in pre-nol biofuel/gasoline blends. *Fuel* 2019;239:1143–8.
- Dagaut P, Togbé C. Experimental and modeling study of the kinetics of oxidation of ethanol-n-heptane mixtures in a jet-stirred reactor. *Fuel* 2010;89(2):280–6.
- da Silva G, Bozzelli J, Liang L, Farrell J. Ethanol Oxidation: Kinetics of the alpha-Hydroxyethyl Radical + O₂ Reaction. *J Phys Chem A* 2009;113:8923–33.
- Barraza-Botet CL, Wooldridge MS. Combustion chemistry of iso-octane/ethanol blends: Effects on ignition and reaction pathways. *Combust Flame* 2018;188:324–36.
- Somers K, Simmie J, Gillespie F, Conroy C, Black G, Metcalf W, et al. A comprehensive experimental and detailed chemical kinetic modelling study of 2,5-dimethylfuran pyrolysis and oxidation. *Combust Flame* 2013;160:2291–319.
- De Bruycker R, Herbinet O, Carstensen H-H, Battin-Leclerc F, Van Geem KM. Understanding the reactivity of unsaturated alcohols: Experimental and kinetic modeling study of the pyrolysis and oxidation of 3-methyl-2-butenol and 3-methyl-3-butenol. *Combust Flame* 2016;171:237–51.
- Ninnemann E, Kim G, Laich A, Alansour B, Terracciano A, Park S, et al. Co-optima fuels combustion: A comprehensive experimental investigation of pre-nol isomers. *Fuel* 2019;254:115630.
- Westbook C, Pitz W, Mehl M, Glaude P-A, Herbinet O, Bax S, et al. Curran and HJ, "Experimental and Kinetic Modeling Study of 2-Methyl-2-Butene: Allylic Hydrocarbon Kinetics," *J Phys Chem A* 2015;119:7462–80.
- Goodwin D, Speth R, Moffat H, Weber B. Cantera: An object-oriented software toolkit for chemical kinetics, thermodynamics, and transport processes. Version 2.4.0, 2018. [Online]. Available: <https://www.cantera.org>.
- Mehl M, Wagnon S, Tsang K, Kukkadapu G, Pitz W, Westbrook C, et al. A comprehensive detailed kinetic mechanism for the simulation of transportation fuels. 10th U.S. National Combustion Meeting LLNL-CONF-725343. 2017.
- Cheng S, Saggese C, Kang D, Goldsborough SS, Wagnon SW, Kukkadapu G, et al. Autoignition and preliminary heat release of gasoline surrogates and their blends with ethanol at engine-relevant conditions: Experiments and comprehensive kinetic modeling. *Combust Flame* 2021;228:57–77.
- Westbrook C, Sjöberg M, Cernansky N. A new chemical kinetic method of determining RON and MON values for single component and multicomponent mixtures of engine fuels. *Combust Flame* 2018;195:50–62.
- Westbrook CK, Mehl M, Pitz WJ, Sjöberg M. Chemical kinetics of octane sensitivity in a spark-ignition engine. *Combust Flame* 2017;175:2–15.
- Gaussian, Inc., "Gaussian 16," Wallingford, CT, 2016.
- Curtiss L, Redfern P, Raghavachari K. Gaussian-4 theory. *J Chem Phys* 2007;126:084108.
- Somers K, Simmie J. Benchmarking compound methods (CBS-QB3, CBS-APNO, G3, G4, A1BD) against the active thermochemical tables: formation enthalpies of radicals. *J Phys Chem A* 2015;119:8922–33.
- Luchini G, Alegre-Requena J, Funez-Ardois I, Paton R. F1000 Res 2020;9:291.
- Bu L, Ciesielski P, Robichaud D, Kim S, McCormick RFT, Nimlos M. Understanding Trends in Autoignition of Biofuels: Homologous Series of Oxygenated C5 Molecules. *J Phys Chem A* 2017;121:5475–86.
- Messery R, Luecke J, St John P, Etz B, Kim Y, Zigler B, et al. Understanding how chemical structure affects ignition-delay-time ϕ -sensitivity. *Combust Flame* 2021;225:377–87.
- Hunwartz N. Modification of CFR Test Engine Unit to Determine Octane Numbers of Pure Alcohols and Gasoline-Alcohol Blends. *SAE Technical Paper 820002*. 1982.
- National Renewable Energy Laboratory, "Co-Optimization of Fuels and Engine (Co-Optima) Project - Fuel Property Database," [Online]. Available: <https://fuelsdb.nrel.gov/fmi/webd/FuelEngineCoOptimization>. [accessed 2018].
- ASTM Special Publication No. 225: Knocking Characteristics of Pure Hydrocarbons, 1958.
- Pal P, Kolodziej C, Choi S, Som S, Broatch A, Gomez-Soriano J, et al. Development of a virtual CRF engine model for knocking combustion analysis. *SAE Int J Engines* 2018;11:1069–82.
- Lokachari N, Wagnon S, Kukkadapu G, Pitz W, Curran H. Experimental and kinetic modeling study of 3-methyl-2-butenol (prenol) oxidation. *Energy Fuels* 2021.
- Sarathy S, Osswald P, Hansen N, K-H. K. Alcohol combustion chemistry. *Prog Energy Combust Sci* 2014;44:40–102.
- Tao L-S, Kang S, Sun W, Wang J, Liao H, Moshhammer K, et al. A further experimental and modeling study of acetaldehyde combustion kinetics. *Combust Flame* 2018;196:337–50.
- Leplat N, Dagaut P, Togbé C, Vandooren J. Numerical and experimental study of ethanol combustion and oxidation in laminar premixed flames and in jet-stirred reactor. *Combust Flame* 2011;158:705–25.
- Zhang Y, El-Merhubi H, Lefort B, Le Moigne L, Curran H, Keromnes A. Probing the low-temperature chemistry of ethanol via the addition of dimethyl ether. *Combust Flame* 2018;190:74–86.
- Tran L-S, Wang Z, Carstensen H-H, Hemken C, Battin-Leclerc F, Kohse-Hoinghaus K. "Comparative experimental and modeling study of the low- to moderate-temperature oxidation chemistry. and furan," *Combustion and Flame*; 2017. p. 251–69.
- D. Lopez-Pintor and J. Dec, "Experimental evaluation of a gasoline-like fuel blend with high renewable content to simultaneously increase ϕ -sensitivity, RON and octane sensitivity," *Fuel*, submitted.
- Mehl M, Chen J, Pitz WSM, Westbrook C. An Approach for Formulating Surrogates for Gasoline with Application toward a Reduced Surrogate Mechanism for CFD Engine Modeling. *Energy Fuels* 2011;25(11):5215–23.

- [49] Stranic I, Pang G, Hanson R, Golden D, Bowman C. Shock Tube Measurements of the Rate Constant for the Reaction Ethanol + OH. *J Phys Chem A* 2014;118(5): 822–8.
- [50] Zador J, Jasper A, Miller J. The reaction between propene and hydroxyl. *PCCP* 2009;11:11040–53.
- [51] Mohamed S, Monge-Palacios M, Raj Giri B, Khaled F, Liu D, Farooq A, Sarathy M. The Effect of Hydrogen Bonding on the Reactivity of OH Radicals with Prenol and Isoprenol: A Shock Tube and Multi-Structural Torsional Variational Transition State Theory Study,“ submitted.
- [52] Sivaramakrishnan R, Su M, Michael J, Klippenstein S, Harding L, Ruscic B. Rate Constants for the Thermal Decomposition of Ethanol and Its Bimolecular Reactions with OH and D: Reflected Shock Tube and Theoretical Studies. *J Phys Chem A* 2010;114(35):9425–39.
- [53] Simmie J, Metcalfe W. Ab Initio Study of the Decomposition of 2,5-Dimethylfuran. *J Phys Chem* 2011;115:8877–88.
- [54] Rotavera B, Taatjes C. Influence of functional groups on low-temperature combustion chemistry of biofuels. *Prog Energy Combust Sci* 2021;86:100925.
- [55] Sivaramakrishnan R, Su M-C, Michael J, Klippenstein S, Harding L, Ruscic B. Rate constants for the thermal decomposition of ethanol and its bimolecular reactions with OH and D: Reflected shock tube and theoretical studies. *J Phys Chem A* 2010; 114:9425–39.
- [56] Bierbach A, Barnes I, Becker K. Rate coefficients for the gas-phase reactions of hydroxyl radicals with furan, 2-methylfuran, 2-ethylfuran, and 2,5-dimethylfuran at 300K. *Atmos Environ* 1992;26A:813–7.
- [57] Aschmann S, Nishino N, Arey JAR. Kinetics of the Reactions of OH Radicals with 2- and 3-Methylfuran, 2,3- and 2,5-Dimethylfuran, and E- and Z-3-Hexene-2,5-dione, and Products of OH + 2,5-Dimethylfuran. *Environ Sci Technol* 2011;45:1859–65.
- [58] Whelan C, Eble J, Mir Z, Blitz M, Seakins P, Olzmann M, et al. Kinetics of the reactions of hydroxyl radicals with furan and its alkylated derivatives 2-methyl furan and 2,5-dimethylfuran. *J Phys Chem A* 2020;124:7416–26.
- [59] Somers K, Simmie J, Gillespie F, Burke U, Connolly J, Meetcalf W, et al. A high temperature and atmospheric pressure experimental and detailed chemical kinetic modelling study of 2-methyl furan oxidation. *Proc Combust Inst* 2013;34:225–32.